جامعة الملك عبدالله
للعلوم والتقنية
King Abdullah University of
Science and Technology

Full waveform inversion based on scattering angle enrichment with application to real dataset

Item Type	Article
Authors	Wu, Zedong;Alkhalifah, Tariq Ali
Citation	Zhen-dong Zhang*, Yike Liu, and Gerard Schuster (2015) Wave Equation Inversion of Skeletonized SurfaceWaves. SEG Technical Program Expanded Abstracts 2015: pp. 2391-2395. doi: 10.1190/segam2015-5805253.1
Eprint version	Publisher's Version/PDF
DOI	10.1190/segam2015-5922173.1
Publisher	Society of Exploration Geophysicists
Journal	SEG Technical Program Expanded Abstracts 2015
Rights	Archived with thanks to SEG Technical Program Expanded Abstracts 2015
Download date	2024-04-17 16:26:55
Link to Item	http://hdl.handle.net/10754/593151

Downloaded 01/06/16 to 109.171.137.210. Redistribution subject to SEG license or copyright; see Terms of Use at http://library.seg.org/

Full waveform inversion based on scattering angle enrichment with application to real dataset

Zedong Wu and Tariq Alkhalifah ,King Abdullah University of Science and Technology

SUMMARY

Reflected waveform inversion (RWI) provides a method to reduce the nonlinearity of the standard full waveform inversion (FWI). However, the drawback of the existing RWI methods is inability to utilize diving waves and the extra sensitivity to the migrated image. We propose a combined FWI and RWI optimization problem through dividing the velocity into the background and perturbed components. We optimize both the background and perturbed components, as independent parameters. The new objective function is quadratic with respect to the perturbed component, which will reduce the nonlinearity of the optimization problem. Solving this optimization provides a true amplitude image and utilizes the diving waves to update the velocity of the shallow parts. To insure a proper wavenumber continuation, we use an efficient scattering angle filter to direct the inversion at the early stages to direct energy corresponding to large (smooth velocity) scattering angles to the background velocity update and the small (high wavenumber) scattering angles to the perturbed velocity update. This efficient implementation of the filter is fast and requires less memory than the conventional approach based on extended images. Thus, the new FWI procedure updates the background velocity mainly along the wavepath for both diving and reflected waves in the initial stages. At the same time, it updates the perturbation with mainly reflections (filtering out the diving waves). To demonstrate the capability of this method, we apply it to a real 2D marine dataset.

INTRODUCTION

Recently, full waveform inversion (FWI) is gaining considerable attention (Virieux and Operto, 2009) as it promises us high resolution velocity models, and an opportunity to utilize more information from the data (like diving waves). However, the promise comes with a considerable cost and many limitations. Specifically, the objective function of FWI conventionally given by the least square misfit between the observed and modeled data, is far from being smooth or convex, especially for high frequency data and specifically for reflections. To slightly mitigate the reflection data limitation, Xu et al. (2012) and Zhou et al. (2012) developed a method based mainly on the work of Plessix et al. (1995) to invert for smooth velocity models using the modeled reflection energy from an image. We refer to the method as reflection waveform inversion (RWI). Biondi and Almomin (2014) propose to extend the equation, split the velocity into a background and perturbed one, and optimize them with a nested approach. Wu and Alkhalifah (2014) implemented RWI using the spectral method as a wavefield extrapolator and utilized a modified objective function that integrates RWI into FWI. In addition, Alkhalifah (2014) proposed a new scattering angle filter applied to the gradient to help control the wavenumber components injected to the model, which will help us avoid falling in a local minima for FWI or RWI. In (Wu and Alkhalifah, 2015), we propose to split the velocity into background and perturbed components and optimize both simultaneously. In order to fully utilize the features of this method, we suggest a small weight to the gradient of v (background) to enhance the convergence of w (perturbation) at the early stage.

In this abstract, we propose a scattering angle enhancement to the method, which is cheaper and has less memory requirement than the original scattering angle filter. It's also a smooth filter, which is important to avoid Gibb's phenomena. Based on this scattering angle enhancement, we direct the energy corresponding to the large scattering angle components to updating v (background) and small scattering angle to updating w (perturbation) at the early stage.

AN IMPROVED FULL WAVEFORM INVERSION FORMULATION AND ITS GRADIENT

Instead of solving the standard FWI optimization problem, we solve the following more general optimization problem (Wu and Alkhalifah, 2015)

$$\min_{v,w} J(p,q) = \frac{1}{2}||C(p+q)-g||^2_{l^2}, \tag{1}$$

$$s.t.\ Ap = B(v)p + f,\ Aq - B(v)q = B'(v)p \cdot^* w. \tag{2}$$

Here, w which acts as the perturbed velocity is a variable independent of v. In this case, v represents the background velocity during the early stages of the inversion. The operator C constrains the wavefield to the receiver position, p is the wavefield modeled from the source wavelet, q is the wavefield modeled from the perturbations, g is the observed data, $Ap = B(v)p + f$ is the wave equation with the source f and $\cdot^*$ is a multiplication operator applied at each time step. Instead of optimizing only v, which is done in standard FWI and RWI, we optimize both v and w, simultaneously. The gradient with respect to v and w can be obtained with the adjoint state method as

$$\frac{\partial J(p,q)}{\partial v} = I + II + III + IV,\ \frac{\partial J(p,q)}{\partial w} = I. \tag{3}$$

In which,

$$I = <\lambda, B'(v)p>_t,\ II = <\lambda, B'(v)q>_t, \tag{4}$$

$$III = <\lambda, B''(v)p \cdot^* w>_t,\ IV = <\mu, B'(v)p>_t, \tag{5}$$

and $\lambda = (A - B(v))^{-T}(C(p+q)-g)$ is the wavefield propagating backward using the residual at the receiver, $\mu = (A - B(v))^{-T}(B^T(\lambda .* w))$ is the wavefield propagating backward using $B^T(\lambda .* w)$ as source. The operation $<\cdot,\cdot>_t$ represents the cross correlation over time. In the above gradient, I is just the gradient of the standard FWI with the residual given by $C(p+q)-g$, $II+IV$ is similar to the gradient of the standard RWI and III is a correcting term. This additional variable w

© 2015 SEG
DOI http://dx.doi.org/10.1190/segam2015-5922173.1

Downloaded 01/06/16 to 109.171.137.210. Redistribution subject to SEG license or copyright; see Terms of Use at http://library.seg.org/

will help produce most of the reflections in the data and leave the residual attributable to mainly the diving waves for which standard FWI gradient term I will include updates along the wavepath of the diving waves. On the other hand, the RWI terms $II+IV$ will contain updates mainly along the wavepath of reflections. Regardless of the term in the gradient, they all involve cross correlation between two wavefields. According to Alkhalifah (2014), keeping mainly the large scattering angle in the cross correlation provides updates along the wave path. Note as well that the objective function is quadratic with respect to w, which helps maintain the independence of that inversion. Thus, we can use the scattering angle filter to insure that only wave path information is admitted to the velocity from the FWI and RWI components in the early stages. The same scattering angle filter can also force only high wavenumber components to be admitted to w by filtering out the high angles.

EFFICIENT SCATTERING ANGLE DECOMPOSITION

Let us denote $I(x)$ as one of the components of the above gradient (4), which is the cross correlation of two wavefields, for example u_s and u_r. That is $I(x)=\int_t u_s(x,t)u_r(x,t)dt$. Here u_s and u_r are an arbitrary forward and adjoint propagating wavefields in equation (4). The time-shift version of $I(x)$, which can be used to access scattering angle information, is defined as

$$I(x,\tau) = \int_t u_s(x,t-\tau)u_r(x,t+\tau)dt \quad (6)$$

$$= \int_{\omega_t} \tilde{I}(x,\omega_t)e^{2i\omega_t\tau}d\omega_t, \quad (7)$$

where we utilize the fact that $\tilde{I}(x,\omega_t)=\hat{u}_s(x,\omega_t)\bar{\hat{u}}_r(x,\omega_t)$ is the cross correlation at the frequency ω_t. The symbol $\hat{\cdot}$ is the Fourier transform in time and $\bar{\cdot}$ is the complex conjugate operator. As defined above, $I(x)=I(x,0)=\int_{\omega_\tau}\int_{k_x}\hat{I}(k_x,\omega_\tau)e^{ik_x\cdot x}dk_xd\omega_\tau$, the exact gradient, is the summation over all the frequencies and wavenumbers. Thus, the scattering angle θ between u_s and u_r satisfies $\frac{|k_x|v}{|\omega_\tau|}=\cos(\theta)$ (Sava and Fomel, 2006). To apply a scattering angle filter, we define an enhanced gradient given by

$$I^n_f(x) = \int_{\omega_\tau}\int_{k_x}\cos^n(\theta)\hat{I}(k_x,\omega_\tau)e^{ik_x\cdot x}dk_xd\omega_\tau \quad (8)$$

$$= v^n\int_{\omega_\tau}\int_{k_x}\frac{|k_x|^n}{|\omega_\tau|^n}\hat{I}(k_x,\omega_\tau)e^{ik_x\cdot x}dk_xd\omega_\tau, \quad (9)$$

$$= v^n\int_\tau\int_{k_x}|k_x|^n e^{ik_x\cdot x}\int_y I(y,\tau)\left(\int_{\omega_\tau}\frac{e^{-i\tau\omega_\tau}}{\omega^n_\tau}\right)e^{-ik_x\cdot y} \quad (10)$$

$$= v^n\int_{k_x}\int_{\omega_t}\frac{|k_x|^n}{\omega^n_t}\hat{\tilde{I}}(k_x,\omega_t)e^{ik_x\cdot x}. \quad (11)$$

Equation (11) is different from equation (8). Implementing equations (8) requires the calculation of $I(x,\tau)$ explicitly, which means more storage and computation time, while equation (11) doesn't require that. In the new formulation, we only need to store the wavefield at several frequencies. In our implementation, we assume that there are no data at frequency $\omega_t=0$

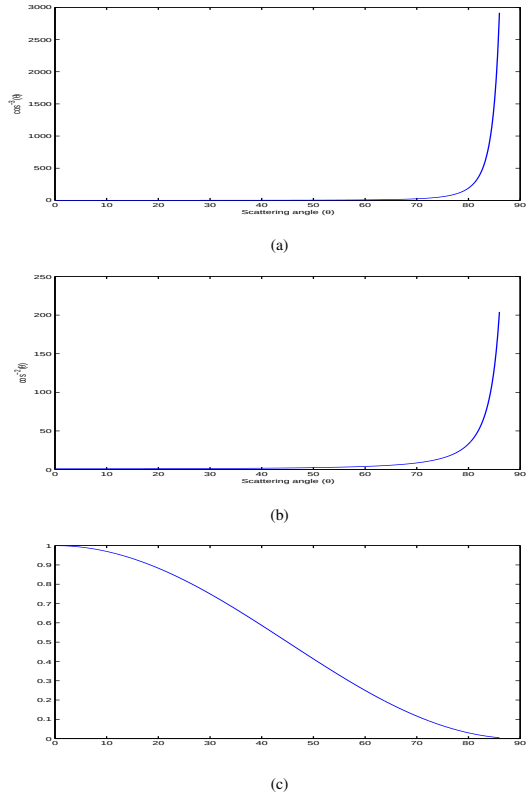

Figure 1: Plots of $cos^{-3}(\theta)$ (a), $cos^{-2}(\theta)$ (b) and $\cos^2(\theta)$ (c).

and set $k_0=k_{minimum}=\frac{\pi}{L_x}$ to avoid the singularity of k, where L_x is the diameter of the domain. Figure 1a, 1b and 1c shows the $cos^{-3}(\theta)$, $\cos^{-2}(\theta)$ and $cos^2(\theta)$ functions as filters to the scattering angle in a reasonable range of θ, in which $\cos(\theta)\in[0.07,1]$. For $n<0$, this operator will enhance the large scattering angles. Smaller n values enhance the large scattering angle even more. For $n>0$, the function enhances the small scattering angle. It's a smooth enhancement for the gradient, which is important to avoid the Gibb's effects. Also, there is a factor v^n weight outside. Typically for the Earth, velocity increases from shallow to deep. This formulation will emphasize the shallower (deeper) part update when $n<0$ ($n>0$) automatically.

For an improved FWI implementation, we use very small $n<0$ to enhance the gradient with respect to v and very large $n>0$ for the gradient with respect to w. For our numerical implementation, we choose $n=2$ for updating w (which is equivalent to the Laplacian filter without the velocity factor) and apply the scattering angle enhancement with $n=-3,\ -2,\ -1,\ 0$ to the gradient with respect to v to update the large scattering angle mainly first, for simplicity.

APPLICATION TO A REAL 2D DATASET

Now, we apply the above described approach on a real 2D marine dataset acquired with a variable depth cable (Soubaras

© 2015 SEG
DOI http://dx.doi.org/10.1190/segam2015-5922173.1

Downloaded 01/06/16 to 109.171.137.210. Redistribution subject to SEG license or copyright; see Terms of Use at http://library.seg.org/

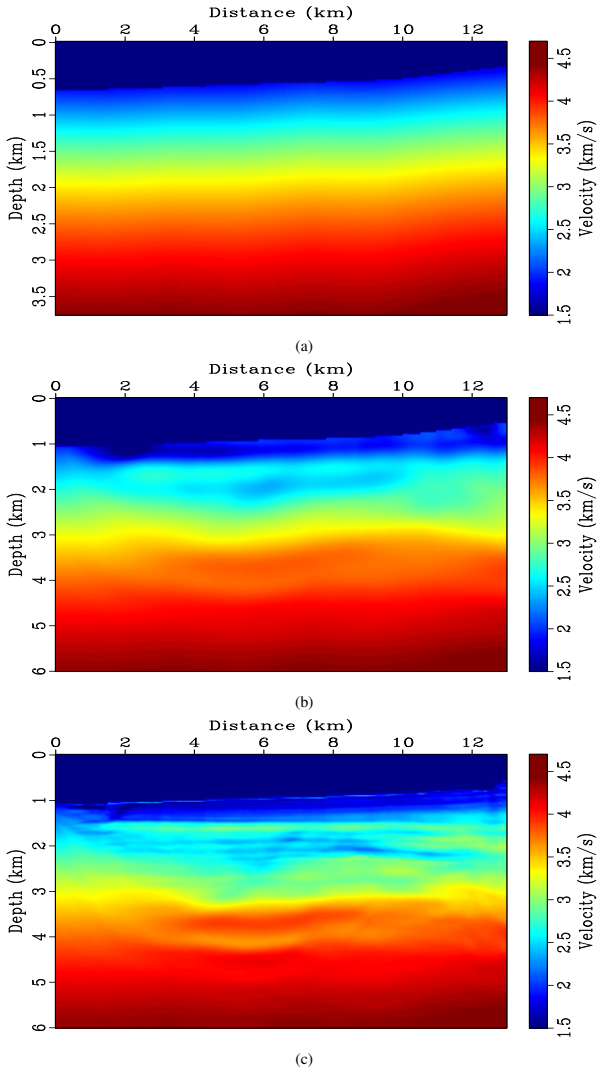

Figure 2: (a) The initial velocity. (b) The inverted velocity using the data corresponding to frequencies less than 3 Hz. (c) The inverted velocity starting from (b) with sequential waveform inversion.

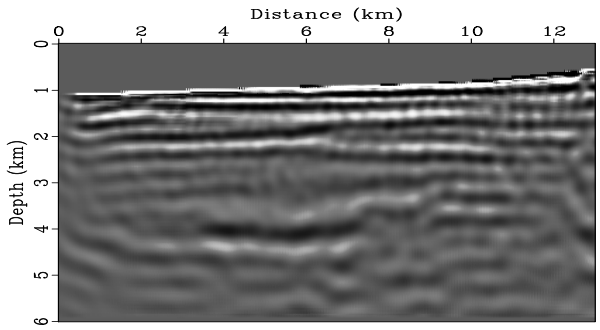

Figure 3: The inverted w using the data energy corresponding to frequencies less than 3 Hz.

and Dowle, 2010). Specifically, the data was acquired with a variable depth streamer, which gives a broader bandwidth through receiver depth notch diversity than conventional flat towed streamer. The increasing cable depths at the intermediate and far offsets, in this case down to 50 m, also boosts the low frequency content which is very helpful for waveform inversion.

Following Díaz et al. (2014), we first average the offset and depth of the receiver of all the shots to reduce the noise. The original dataset has 1824 shots with 18.75 m shot interval. The minimum offset is 169 m, while the receiver interval is 12.5 m. The maximum recording time is about 7 s. We choose one shot in every four and a total 200 shots in our inversion to reduce the cost. The initial model is obtained by converting the stacking velocity to interval velocity (Dix, 1955) with proper smoothing, followed by time-to-depth conversion. After that, we do a reverse time migration (RTM) with a constant velocity 1.5 km/s to obtain a rough water bottom. We set the initial velocity in the water layer to the water velocity of 1.5 km/s and keep it fixed throughout the inversion. The resulting initial velocity model is shown in Figure 2a. Figure 4a shows the corresponding RTM image. The angle gather from 0 to 45^o obtained using the space shift imaging condition (Sava and Fomel, 2003) is shown in Figure 5a. Note that we do not use the angle gathers in the inversion; instead, we use these particular gathers as an independent quality control test. The moveout in the gathers confirms that the velocity is too fast. We first filtered out of the data frequencies larger than 3 Hz and apply the new scattering angle filtering based Full waveform inversion with $n = -3, -2, -1, 0$. Before each full waveform inversion, we invert the source wavelet. The inversion is implemented on a space sampling of 40 m in depth and 18.75 m in the x direction. Since the receiver is not located on the grid, we apply a linear interpolation to obtain the modeled data. The resulting velocity from this low frequency inversion is shown in Figure 2b. After that we sequentially apply the standard Full waveform inversion with the data obtained by filtering out the frequency larger than 4, 5, 6, 8, 10 and 15 Hz. At last, we obtain the inverted velocity as shown in Figure 2c. The RTM result with the inverted velocity (Figure 2c) is shown in Figure 4b. The corresponding angle gathers are shown in Figure 5b. The angle gathers (Figure 5b) obtained from the RTM using the inverted velocity model is flatter than that (Figure 5a) corresponding to the initial velocity model. It shows that the inverted velocity model is better for prestack depth migration. The comparison of the RTM results indicate that the image in Figure 4b is better focused than the image in Figure 4b. Figure 6a and Figure 6b compares the shot gathers corresponding to shot 100 of the original data and the one modeled from the inverted velocity. This comparison clearly demonstrates the parts of the data we managed to fit. Considering we are applying an acoustic inversion to a mostly elastic Earth, we expect to have discrepancies in the data fit. However, we clearly managed to reproduce some of the shallow reflections.

© 2015 SEG
DOI http://dx.doi.org/10.1190/segam2015-5922173.1

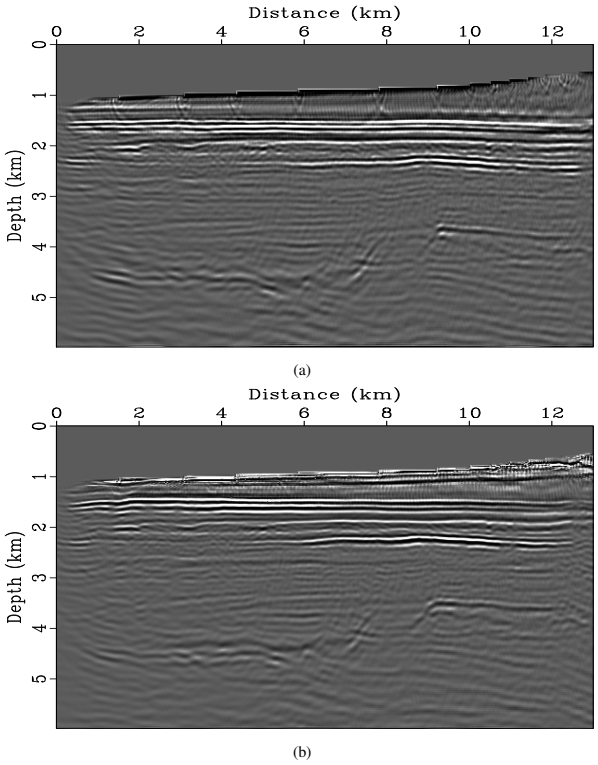

Figure 4: The reverse time migration result obtained using the initial velocity (a) and the inverted one (b).

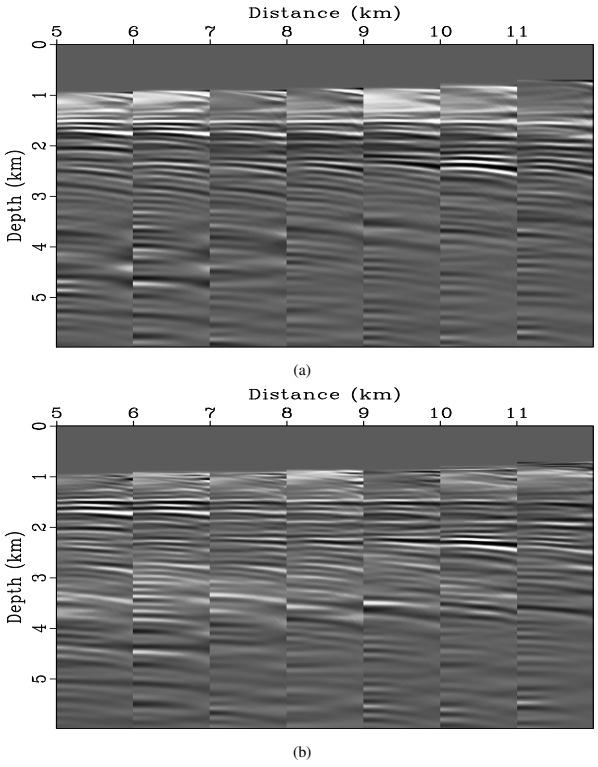

Figure 5: The angle gather obtained from initial velocity (a) and inverted one (b).

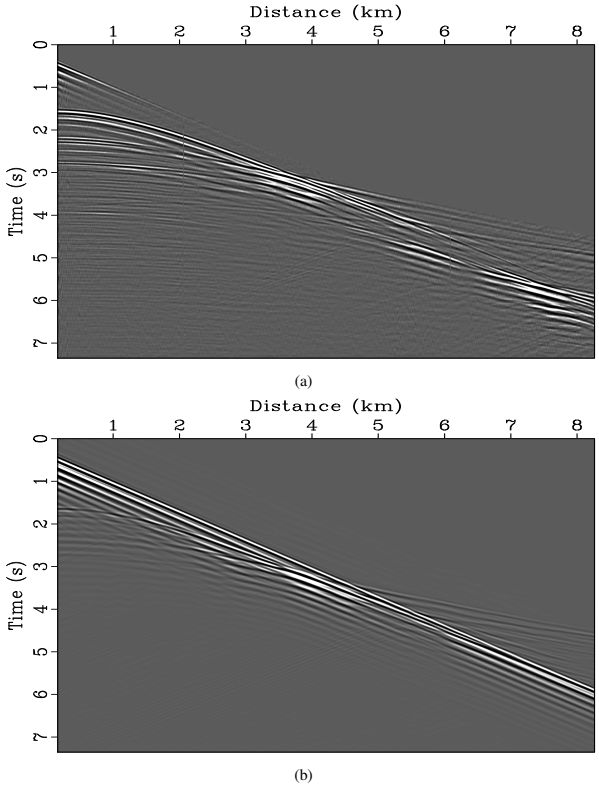

Figure 6: The seismogram comparison of the recorded data (a) and the modeled one (b) using the inverted velocity.

CONCLUSIONS

We solve a new optimization problem that measures the misfit between the observed and the modeled data from the source and from the image and inverts for both the background velocity and the perturbation (equivalent to the image in action), simultaneously. We derive a new scattering angle filter and apply it to enhance the energy corresponding to the large scattering angles in updating velocity and the small scattering angles in updating the perturbation, which updates v mainly with the tomographic components, and w absorbs the reflected components, at the initial stages. An application to a real dataset shows that the proposed method can handle complicated velocity models. The angle gather comparison shows that the algorithm can improve the migration velocity for prestack depth migration.

ACKNOWLEDGEMENTS

We thank Bruce VerWest and Esteban Díaz for their insights in the CGG data. The seismic data shown in this abstract is proprietary to and provided courtesy of CGG. We thank KAUST for its support and we thank the SWAG group for collaborative environment.

Downloaded 01/06/16 to 109.171.137.210. Redistribution subject to SEG license or copyright; see Terms of Use at http://library.seg.org/

© 2015 SEG
DOI http://dx.doi.org/10.1190/segam2015-5922173.1

Downloaded 01/06/16 to 109.171.137.210. Redistribution subject to SEG license or copyright; see Terms of Use at http://library.seg.org/

EDITED REFERENCES

Note: This reference list is a copyedited version of the reference list submitted by the author. Reference lists for the 2015 SEG Technical Program Expanded Abstracts have been copyedited so that references provided with the online metadata for each paper will achieve a high degree of linking to cited sources that appear on the Web.

REFERENCES

Alkhalifah, T., 2014, Scattering-angle based filtering of the waveform inversion gradients: Geophysical Journal International, **200**, no. 1, 363–373. http://dx.doi.org/10.1093/gji/ggu379.

Biondi, B., and A. Almomin, 2014, Simultaneous inversion of full data bandwidth by tomographic full-waveform inversion: Geophysics, **79**, no. 3, WA129–WA140. http://dx.doi.org/10.1190/geo2013-0340.1.

Diaz, D., E. Y. Duan, P. Sava, and G. Pratt, 2014, Image-domain and data-domain waveform tomography: A case study: 84th Annual International Meeting, **236**, 1243–1248.

Dix, C. H., 1955, Seismic velocities from surface measurements: Geophysics, **20**, 68–86. http://dx.doi.org/10.1190/1.1438126.

Plessix, R., Y. De Roeck, and G. Chavent, 1995, Automatic and simultaneous migration velocity analysis and waveform inversion of real data using an MBTT/WKBJ formulation: Presented at the 75th Annual International Meeting, SEG.

Sava, P., and S. Fomel, 2006, Time-shift imaging condition in seismic migration: Geophysics, **71**, no. 6, S209–S217. http://dx.doi.org/10.1190/1.2338824.

Sava, P. C., and S. Fomel, 2003, Angle-domain common-image gathers by wavefield continuation methods: Geophysics, **68**, 1065–1074. http://dx.doi.org/10.1190/1.1581078.

Soubaras, R., and R. Dowle, 2010, Variable-depth streamer — A broadband marine solution: First Break, **28**.

Virieux, J., and S. Operto, 2009, An overview of full-waveform inversion in exploration geophysics: Geophysics, **74**, no. 6, WCC1–WCC26. http://dx.doi.org/10.1190/1.3238367.

Wu, Z., and T. Alkhalifah, 2014, Spectral implementation of full-waveform inversion based on reflections: 76th Annual International Conference and Exhibition, EAGE Extended Abstracts, http://dx.doi.org/10.3997/2214-4609.20140853.

Wu, Z., and T. Alkhalifah, 2015, Simultaneous inversion of the background velocity and the perturbation in full-waveform inversion: Presented at the 77th Annual International Conference and Exhibition, EAGE.

Xu, S., D. Wang, F. Chen, G. Lambare, and Y. Zhang, 2012, Inversion on reflected seismic wave: 82nd Annual International Meeting, SEG, Expanded Abstracts, http://dx.doi.org/10.1190/segam2012-1473.1.

Zhou, H., L. Amundsen, and G. Zhang, 2012, Fundamental issues in full-waveform inversion: Presented at the 82nd Annual International Meeting, SEG, Expanded Abstracts, http://dx.doi.org/10.1190/segam2012-0878.1.